

The historical origins of the so-called *low-Froude* or *low-Speed paradox* that forms the subject of this chapter is often attributed to the work of naval architect T. F. Ogilvie [Ogilvie, 1968] — although Ogilvie cites the earlier work of Nils Salvesen [Salvesen, 1966, 1969] as providing the initial paradox.

Let us consider the surface waves produced by a body moving within or beneath a free surface under the effects of gravity. A prototypical situation is shown below:

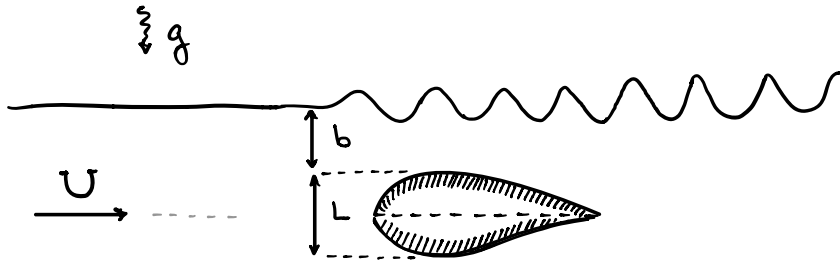


Figure 12.1: Flow past an aerofoil

Previously, Michell [1898] proposed the idea of a thin-ship approximation, in which the solution is approximated under the assumption that the obstruction is thin in one or several of its dimensions. For the above situation, the free surface height,  $\eta(x)$ , can be expanded as

$$\eta(x) = \eta_0(x) + \delta\eta_1(x) + \delta^2\eta_2(x) + \dots \quad (12.1)$$

where  $\delta = L/b \ll 1$  characterises the thinness of the obstruction in comparison with its depth of submergence. The boldness and ingenuity of Michell’s approximation was twenty-years beyond the state-of-the-art [Tulin, 1978, Wehausen, 1973]; it went unappreciated until the expansion by Havelock [1923]. Much later, Tuck [1965] studied the linear ship-wave theory of Michell, and indicated that the second-order thin-ship approximation was contentious because it invalidated the surface boundary conditions — thus Michell’s procedure does not preserve the free surface as a streamline of the flow.

Consequently, during this period of the 1960s and 1970s, there was great interest in better understanding the higher-order approximations of ship-wave theory. In view of this, Salvesen [1966] performed a numerical and experimental study of flow past a submerged aerofoil. Michell’s approximation was computed to third order, and Salvesen produced the graph in fig. 12.2, which demonstrates how each term in the approximation contributes to estimating the downstream wave height. The key aspect of fig. 12.2 is that the relative contribution of the third-order effects (shown solid) [*i.e.*  $\delta^3\eta_3/(\eta_0 + \delta\eta_1 + \delta^2\eta_2)$  in relation to (12.1)] exceeds the contributions from the first- and second-order effects when the speed,  $U$ , is continually diminished.

Figure 12.2: A reproduction of Salvesen's figure from Salvesen [1969] showing a comparison of downstream wave heights using first- (dash-dotted), second- (dashed), and third-order (solid) thin-ship theory. The higher-order contributions are more important as  $U \rightarrow 0$ .

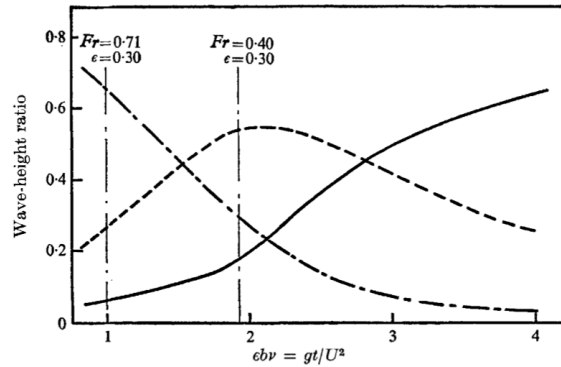


FIGURE 5. First-, second- and third-order wave heights at low speeds. —.—,  $H^{(1)}/(H^{(1)}+H^{(2)}+H^{(3)})$ ; ---,  $H^{(2)}/(H^{(1)}+H^{(2)}+H^{(3)})$ ; —,  $H^{(3)}/(H^{(1)}+H^{(2)}+H^{(3)})$ .

For the two-dimensional wave-structure interactions typified by fig. 12.1, the Froude number,

$$\text{Fr} = \frac{U}{\sqrt{gL}},$$

provides a relative measure of the inertial effects in comparison to gravitational effects. The above is for a flow with characteristic velocity,  $U$ , length scale  $L$ , and gravity  $g$ .

Salvesen's work, and the unusual behaviour of the series approximations in the low-Froude limit was highlighted by Ogilvie [1968]:

*It appears paradoxical that it should be necessary to include higher-order approximations at very low speeds, for the total disturbance becomes small and smaller as speed is reduced more and more toward zero. One should expect that the assumptions required for linearizing ought to become steadily more nearly valid as the free-surface deflection decreases. Instead, the problem appears to become more nonlinear!*

At the time it was understood that the perturbative problem of  $\text{Fr} \rightarrow 0$  was singular and in this limit, the resultant free-surface waves are exponentially small in the Froude number. However, this initiated a longstanding search for a consistent low-Froude theory. The history of the low-Froude problem from a naval standpoint is summarised by Tulin [2005, 1978]. Work in this area continued through Ogilvie and colleagues (Ogilvie 1968, 1970, Ogilvie and Chen 1982, Chen and Ogilvie 1982), but also through a variety of international efforts. Perhaps the first paper to relate the low-Froude problem to beyond-all-orders techniques was the semi-numerical work by Vanden-Broeck et al. [1978] on two-dimensional blunt-bodied, and there are further important ideas using the ray-theoretic viewpoint of geometrical optics by Keller [1978].

The first exponential asymptotics of the low-Froude problem appears in Chapman and Vanden-Broeck [2002] (for capillary waves) and Chapman and Vanden-Broeck [2006] (for gravity waves), and in recent years, this has initiated a great number of interesting extensions. Our work in this chapter will follow the latter approach.

## 12.1 WATER WAVE EQUATIONS AS AN INTEGRO-DIFFERENTIAL EQUATION

Let us consider two-dimensional steady irrotational flow past a semi-infinite body, which consists of a flat bottom ( $y = -H$ ,  $x < 0$ ), and a face oriented at an angle  $\pi\sigma$  to the horizontal ( $0 < \sigma < 1$ ). There is a uniform stream of speed  $U$  as  $x \rightarrow -\infty$ , and we assume that the flow attaches to the stern at a stagnation point. So the situation looks like the below.

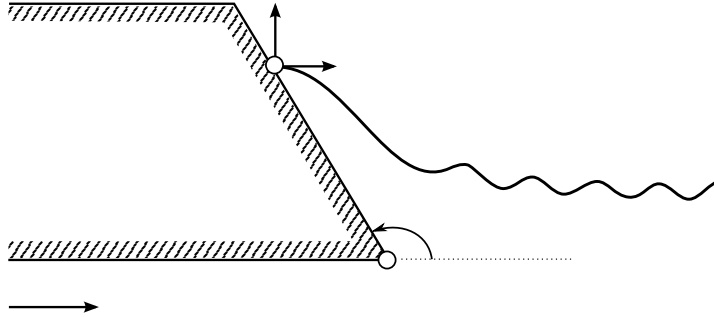


Figure 12.3: Physical flow past a ship

We let  $\mathbf{u} = [u(x, y), v(x, y)]$  be the velocity at a point in the fluid. The velocity potential is introduced, with  $\mathbf{u} = \nabla\phi(x, y)$ . The problem can be non-dimensionalised<sup>1</sup>. The motion of the fluid [see [Vanden-Broeck \[2010\]](#)] is then governed by Laplace's equation, with the kinematic condition on all boundaries, and Bernoulli's equation on the free-surface:

$$\nabla^2\phi = 0 \quad \text{for } (x, y) \text{ in the fluid,} \quad (12.2a)$$

$$\frac{\partial\phi}{\partial n} = 0 \quad \text{for } (x, y) \text{ on the hull and free-surface,} \quad (12.2b)$$

$$\frac{\epsilon}{2}|\nabla\phi|^2 + y = 0 \quad \text{for } (x, y) \text{ on the free-surface,} \quad (12.2c)$$

where all variables now non-dimensional. The parameter  $\epsilon = U^2/gL$  is related to the square of the draft-based Froude number and  $\epsilon \ll 1$  is the low-Froude regime we shall study.

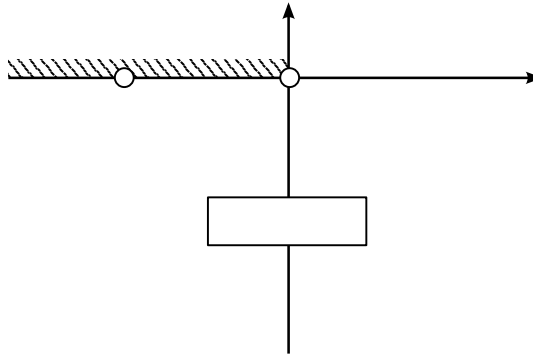
The solution of (12.2) is difficult primarily for two reasons. First, the flow domain is relatively complicated—here, the normal derivative conditions must be applied along the stern body as well as an unknown free-surface. Second, the dynamic condition (12.2c) is nonlinear. In modern day computation, we would typically need to mesh the flow domain and solve the partial differential equation numerically using finite-difference or finite-element schemes.

However, in two-dimensional potential flows, complex variable theory can be applied to reformulate the problem in a more tractable form. The trick is to introduce the complex potential  $w = \phi + i\psi$ , which combines the potential  $\phi$  with its harmonic conjugate, the streamfunction,  $\psi$ . We also set  $z = x + iy$ . The role of the dependent and independent variables are then switched, and we seek  $z = z(w)$ . The ship/free-surface lying along ABC is a streamline of the flow, and can be chosen to be  $\psi = 0$ . If  $z(w)$  is analytic in the fluid region, then Laplace's equation (12.2a)

We give a very basic introduction to the development of the boundary-integral formulation of potential flow suitable for those without a background in fluid mechanics.

<sup>1</sup>Non-dimensionalisation is the procedure in which variables are scaled according to typical physical lengths; here (i) the stagnation point is located at  $(x, y) = (0, 0)$  and  $\phi = 0$ ; (ii) the corner of the stern is located at  $\phi = -1$ ; and (iii) the potential tends to the unit free-stream,  $\phi \rightarrow 1$ , as  $x \rightarrow -\infty$

is satisfied. Similarly, as the boundary lies on  $\psi = 0$ , the kinematic condition (12.2b) is satisfied.



Instead of solving for  $z(w)$ , we shall find it more convenient to work with speed and angular components. We introduce  $q$  for the speed of the flow and  $\theta$  for the angle the streamline makes with the  $x$ -axis. Then

$$qe^{-i\theta} \equiv \frac{dw}{dz} = u - iv, \quad (12.3)$$

The imposition of Laplace's equation  $\nabla^2\phi = 0$  is then equivalent to imposing a boundary-integral relationship that relates  $q$  and  $\theta$ . By Cauchy's theorem, this relationship is shown to be

$$\log q = \frac{1}{\pi} \int_{-\infty}^{\infty} \frac{\theta(\varphi)}{\varphi - \phi} d\varphi.$$

<sup>2</sup>The Cauchy Principal Value Integral is defined via  $\int_{-\infty}^{\infty} \dots d\varphi = \lim_{\delta \rightarrow 0} (\int_{-\infty}^{\phi-\delta} + \int_{\phi+\delta}^{\infty}) \dots d\varphi$ .

The 'dash' through the integral signifies the Cauchy Principal Value<sup>2</sup>. The key is that we have replaced the two-dimensional Laplace's equation,  $\nabla^2\phi = 0$ , with an integral equation that only requires values on  $\psi = 0$ .

Imposing the hull geometry<sup>3</sup> and setting  $\theta = 0$  for  $\phi < -1$  and  $\theta = \pi\sigma$  for  $-1 < \phi < 0$  then gives

$$\log q = \log \left( \frac{\phi}{\phi + 1} \right)^\sigma + \frac{1}{\pi} \int_0^\infty \frac{\theta(\varphi)}{\varphi - \phi} d\varphi. \quad (12.4)$$

<sup>3</sup>Note that the relation between  $\phi$  and the physical plane (and hence the physical size of the ship's face) can be determined *a posteriori* once (12.5) and (12.4) have been solved.

Differentiating Bernoulli's equation (12.2c) tangentially, that is, with respect to  $\phi$ , yields

$$\epsilon q^2 \frac{dq}{d\phi} + \sin \theta = 0, \quad (12.5)$$

where the free surface condition is applied to the streamline  $\psi = 0$  for  $\phi > 0$ .

The task is to solve for the two unknowns  $q(\phi)$  and  $\theta(\phi)$  along the physical free surface,  $\phi > 0$ . Once this is done, the physical coordinates can be obtained by integrating (12.3), theta is

$$z(\phi) = x(\phi) + iy(\phi) = \int_0^\phi \frac{e^{i\theta(\varphi)}}{q(\varphi)} d\varphi.$$

```

% Parameters and potential mesh
n = 1000; dw = 0.03; ep = 1; sigma = 1/2;
phi = (0:n-1)*dw; phim = phi(1:end-1) + dw/2;

% Solve the system and plot the solution
fwd = @(u)func(u, phi, phim, n, ep, sigma, dw);
theta = fsolve(fwd, zeros(1, n)); [F,tau_m] = fwd(theta);
qm = exp(tau_m);
plot(phim, qm); xlabel('\phi'); ylabel('q');

function [F,tau] = func(u, w, wm, n, ep, sigma, dw)
% Function file for Bernoulli's equation
tau = sigma*log(wm./(wm+1)); aux = [dw*ones(1,n-1) dw/2];
for j = 1:n-1, tau(j) = tau(j) + 1/pi*sum(u.*aux./(w-wm(j)));
end

thetam = 1/2*(u(1:n-1)+u(2:n));
dtau = 1/dw*((tau(2)-tau(1)), ...
(tau(3:n-1)-tau(1:n-3))/2.0, (tau(n-1)-tau(n-2)));

F(1:n-1) = ep*exp(2*tau).*dtau + exp(-tau).*sin(thetam);
F(n) = u(1);
end

```

Table 12.1: This MATLAB code solves for the ship stern problem. This particular instance solves the  $\sigma = 0.5$  stern at  $\epsilon = 1.0$  with  $n = 1000$  points and a discretisation distance of  $\Delta\phi = 0.03$  (denoted  $dw$  in the code). It makes use of MATLAB's `fsolve` function for the solution of the algebraic equation denoted by `func`.

## 12.2 NUMERICAL SOLUTIONS OF THE STERN PROBLEM

Our task is to solve for the speed,  $q$ , and angle  $\theta$  along the free surface,  $\phi > 0$ . We have a nonlinear differential equation (12.5) as well as a boundary-integral relationship (12.4). This can be done using the following simple algorithm<sup>4</sup>.

We first truncate the semi-infinite domain to a finite interval and introduce an equally spaced mesh<sup>5</sup> for  $\phi = \phi_i$  with  $i = 1, \dots, n-1$ . We also define the midpoints  $\phi_i^m$  for  $i = 1, \dots, n-1$ , which are introduced as a device to avoid the singular nature of the integral. The midpoint values of  $\tau_i^m = \log q_i^m$  are calculated from the integral (12.4). The principal value integral is computed by applying the trapezoidal rule with a summation over the mesh points  $\phi_i$ ; this use of equally spaced points and midpoints should allow us to neglect the singularity of the principal value without losing accuracy.

Bernoulli's equation, evaluated at the midpoint values, then provides a system of  $n-1$  equations to solve. The derivatives  $d\tau/d\phi$  are computed using second-order differences. For the  $n^{\text{th}}$  equation, we assign the boundary condition corresponding to a stagnation point,  $F_n = \theta_1 = 0$

Table 12.1 shows just how compact this code can be made when combined with the built-in nonlinear solver of the MATLAB environment. In the included example, we solve for the vertical  $\sigma = 1/2$  hull at  $\epsilon = 0.8$ . An example output is shown in fig. 12.4.

## 12.3 NAIVE ASYMPTOTIC ANALYSIS

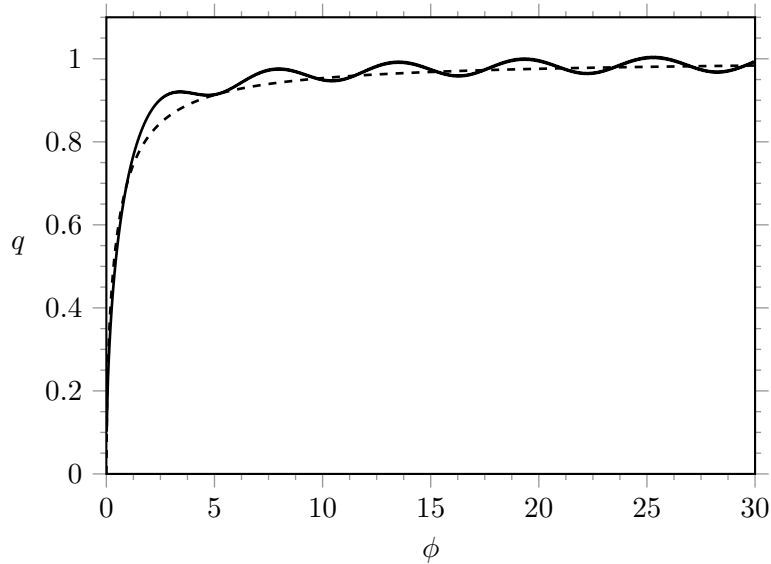
In the naive analysis, we would expand  $q$  and  $\theta$  as series expansions in powers of  $\epsilon$ . Setting  $q = q_0 + \epsilon q_1 + \dots$  and  $\theta = \theta_0 + \epsilon \theta_1 + \dots$ , then from the surface equation (12.5), we have  $\sin \theta_0 = 0$  and hence  $\theta_0 = 0$ . Indeed this is a sensible approximation – as  $\epsilon \rightarrow 0$ , the speed of the stream tends to zero and the free-surface is approximately flat<sup>6</sup>. If we

<sup>4</sup>These methodologies are used by many authors computing two-dimensional nonlinear flows over obstructions; more details can be found in the general reference by Vanden-Broeck [2010].

<sup>5</sup>The main points are  $\phi_i = (i-1)\Delta\phi$  with separation distance  $\Delta\phi$  for  $i = 1, \dots, n$  and the midpoints are  $\phi_i^m = \frac{1}{2}(\phi_i + \phi_{i+1})$  for  $i = 1, \dots, n-1$ .

<sup>6</sup>Alternatively we can consider  $\epsilon \rightarrow 0$  as equivalent to taking gravity,  $g \rightarrow \infty$ , which has the effect of pressing the surface flat

Figure 12.4: Solution for  $\sigma = 1/2$  at  $\epsilon = 0.8$  (solid), computed using the code in 12.1. The leading-order asymptotic approximation is shown dashed.



now substitute  $\theta_0 = 0$  into (12.4) we obtain the leading-order speed on the free-surface,

$$q_0 = \left( \frac{\phi}{\phi + 1} \right)^\sigma. \quad (12.6)$$

The above leading-order speed has been plotted in fig. 12.4, where we see it agrees very well with the solution—except for the fact it fails to capture the surface waves. The above solution is known as the ‘double-body flow’ since it is akin to flow over the step and the ‘image of the step’ within a rectangular channel<sup>7</sup>.

<sup>7</sup>Need a picture

Notice, as well, that the analytic continuation of  $q_0$  from the physical free surface, where  $\phi > 0$ , and into the complex  $\phi$ -plane, yields a singularity at  $\phi = -1$  or more generally, at  $\phi = e^{\pm\pi i}, e^{\pm 3\pi i}, \dots$ . The next order in (12.5), shows that

$$\theta_1 = -q_0^2 \frac{dq_0}{d\phi}, \quad (12.7)$$

and consequently,  $\theta_1$  (and  $q_1$ ) will inherit the branch point singularities in  $q_0$ . Each order differentiates the previous, and hence the power of the singularity must grow. The series diverges and the task now is to characterise this divergence.

#### 12.4 ASYMPTOTIC ANALYSIS AS $n \rightarrow \infty$

As we have noted, the singularity at  $\phi = -1$  (and possibly  $\phi = 0$ ) in (12.6) drives the divergence of the asymptotic expansion. Such singularities are typically complex-valued and lie away from the physical domain. Thus, to study their effects, we must consider an extension of the governing equations to the complex plane. Let  $\phi$  be complex and we label<sup>8</sup>  $\phi = \phi_r + i\phi_c \mapsto w \in \mathbb{C}$ . We now have

<sup>8</sup>There is a somewhat confusing abuse of notation where we have relabeled the complexified  $\phi$  as the former complex potential variable,  $w$ .

$$\log q \pm i\theta = \log\left(\frac{w}{w+1}\right)^\sigma + \hat{\mathcal{H}}\theta, \quad (12.8a)$$

$$\epsilon q^2 \frac{dq}{dw} + \sin\theta = 0, \quad (12.8b)$$

where we have defined  $\hat{\mathcal{H}}$  to be the complex Hilbert transform operator<sup>9</sup>,

$$\hat{\mathcal{H}}\theta(w) = \frac{1}{\pi} \int_0^\infty \frac{\theta(\varphi)}{\varphi - w} d\varphi.$$

The  $\pm$  sign that appears in the integral equation corresponds to analytic continuation in the upper and lower half- $w$ -planes, respectively, and we can verify that as  $w$  approaches the positive real axis, we recover the previous real-valued formulation.<sup>10</sup> In the following, we shall perform the study for analytic continuation into the upper half-plane.

We substitute

$$q = \sum_{n=0}^\infty \epsilon^n q_n \quad \text{and} \quad \theta = \sum_{n=0}^\infty \epsilon^n \theta_n. \quad (12.9)$$

into (12.8). This yields for the first two orders,

$$\theta_0 = 0 \quad \text{on } w \in \mathbb{R}^+, \quad (12.10a)$$

$$q_0 = \left(\frac{w}{w+1}\right)^\sigma, \quad (12.10b)$$

$$\theta_1 = -q_0^2 \frac{dq_0}{dw}, \quad (12.10c)$$

$$\frac{q_1}{q_0} + i\theta_1 = \hat{\mathcal{H}}\theta_1(w). \quad (12.10d)$$

The full expressions for the higher  $\mathcal{O}(\epsilon^n)$  terms are more complicated, but there is significant simplification as  $n \rightarrow \infty$ . Examining  $q_0$  in (12.10b), the solution contains two singularities, identifiable with points in the flow-domain—one at the corner of the stern ( $w = -1$ ) and the other at the stagnation point ( $w = 0$ ). Because all the higher-order problems are linear, no new singularities can be introduced and thus the singular points of  $q_n(w)$  must be those same singularities as for  $q_0$ . Then as  $n \rightarrow \infty$ , we can expect the late terms to behave like factorial over power,

$$\theta_n \sim \frac{\Theta(w)\Gamma(n+\gamma)}{\chi(w)^{n+\gamma}} \quad \text{and} \quad q_n \sim \frac{Q(w)\Gamma(n+\gamma)}{\chi(w)^{n+\gamma}}. \quad (12.11)$$

The relevant terms<sup>11</sup> at  $\mathcal{O}(\epsilon^n)$  are:

$$\underbrace{\frac{q_n}{q_0} + i\theta_n}_{\text{first order}} - \underbrace{\frac{q_{n-1}q_1}{q_0^2}}_{\text{second order}} + \dots = \underbrace{\hat{\mathcal{H}}[\theta_n]}_{\text{exp. subdominant}}, \quad (12.12)$$

$$\underbrace{q_0^2 q'_{n-1}}_{\text{first order}} + \underbrace{2q_0 q_1 q'_{n-2} + 2q_0 q_0' q_{n-1}}_{\text{second order}} + \dots = \underbrace{-\cos(\theta_0)\theta_n}_{\text{first order}} + \dots \quad (12.13)$$

We claim, at least for the moment, that the integral on the right-hand side of the boundary integral equation (12.12) is exponentially

<sup>9</sup>Notice here that for  $w$  in the upper- or lower-half complex plane, the integral no longer requires the principal value.

<sup>10</sup>Specifically, as  $w \rightarrow \phi_r$  from the upper-half plane, we have  $\hat{\mathcal{H}}\theta = \frac{1}{\pi} \int_0^\infty \frac{\theta}{\varphi - \phi_r} d\varphi + i\theta$ . The argument for the lower half-plane is performed analogously with a change in sign of the residue contribution.

<sup>11</sup>In the limit that  $n \rightarrow \infty$ , terms like  $q_m q_n$  (for  $m$  finite) dominate terms with smaller indices in  $n$ , such as  $q_m q_{n-1}$ . Moreover, differentiating a term increases the order (in  $n$ ) by 1, so a term like  $\epsilon dq_{n-1}/dw$  is of the same order as  $q_n$ .

subdominant to the terms on the left-hand side for large  $n$ . We address this claim a little later in §12.8, but for now, we will assume that

$$q_n \sim -iq_0\theta_n - i\theta_{n-1}q_1 + \dots \quad \text{as } n \rightarrow \infty, \quad (12.14)$$

obtained from setting  $\mathcal{H}^\wedge$  to zero in (12.12) and re-arranging.

Finally, substituting (12.14) into the dynamic condition (12.13) and simplifying yields the final form of our  $\mathcal{O}(\epsilon^n)$  expression:

$$\overbrace{\left[ q_0^3 q'_{n-1} + iq_n \right]}^{\text{first/second order}} + \underbrace{\left[ 2q_0^2 q'_0 q_{n-1} + 2q_0^2 q_1 q'_{n-2} - i \frac{q_{n-1} q_1}{q_0} \right]}_{\text{second order}} + \dots = 0. \quad (12.15)$$

At this point, the manipulations are similar to those that appear in previous chapters. The factorial over power ansatz (12.11) is substituted into (12.15) and the first two orders as  $n \rightarrow \infty$  extracted. This yields differential equations for the two key components of  $\chi$  and  $Q$ :

$$\frac{d\chi}{dw} = \frac{i}{q_0^3}, \quad (12.16a)$$

$$\frac{Q'}{Q} = -\frac{2q'_0}{q_0} + \frac{3iq_1}{q_0^4}. \quad (12.16b)$$

Integrating then yields

$$\chi = \int_{w_0}^w \frac{i}{q_0^3(\varphi)} d\varphi, \quad (12.17a)$$

$$Q = \frac{\Lambda}{q_0^2} \exp\left(3i \int_{w^\star}^w \frac{q_1(\varphi)}{q_0^4(\varphi)} d\varphi\right). \quad (12.17b)$$

The function  $\chi$  is assumed to drive the divergence of the asymptotic expansion, with  $\chi = 0$ , at a selected singularity,  $w_0$ . We will choose the initial point of integration in the next section. In the expression for  $Q$ ,  $\Lambda$  is a constant of integration and  $w^\star$  is any arbitrary point for which the integral exists.

By the ansatz (12.11) and the simplification of the boundary-integral relationship in (12.14), we know that  $\theta_n \sim iq_n/q_0$  and thus

$$\Theta = \frac{\Lambda i}{q_0^3} \exp\left(3i \int_{w^\star}^w \frac{q_1(\varphi)}{q_0^4(\varphi)} d\varphi\right). \quad (12.18)$$

Finally, it remains to determine the power,  $\gamma$ , that appears in the ansatz (12.11), as well as the prefactor  $\Lambda$ .

## 12.5 INNER PROBLEM

In order to completely determine the divergent behaviour of (12.11), we must calculate the power  $\gamma$  and prefactor  $\Lambda$ . Firstly,  $\gamma$  can be determined by ensuring that the singularity predicted by the late-orders form is consistent with the singularity present in the low orders. Let us

In general, we may need to consider a sum over multiple ansatzes of the form (12.11) and hence an expression such as  $\sum \frac{Q_k \Gamma(n+\gamma_k)}{\chi_k^{n+\gamma_k}}$ . However, the development of the factorial-over-power ansatzes are typically linear so it suffices to consider an individual one as we do here.

focus on the singularity at  $w = -1$  and define  $W = w + 1$ . By (12.10b), we have that

$$q_0 \sim cW^\alpha \quad \text{as } W \rightarrow 0 \quad (12.19)$$

where  $c = (-1)^\sigma$  and  $\alpha = -\sigma$ . Using the above asymptotic behaviour in (12.17a) and performing a local integration, we have that in the same limit,

$$\chi \sim \frac{W^{1-3\alpha}}{c^3(1-3\alpha)} = \mathcal{O}(W^{1-3\alpha}). \quad (12.20)$$

Similarly, the inner limit of  $Q$  in (12.17b) can be obtained<sup>12</sup> as  $W \rightarrow 0$ , and demonstrates that

$$Q = \mathcal{O}\left(\frac{1}{q_0^5}\right) = \mathcal{O}(W^{-5\alpha}). \quad (12.21)$$

Thus as the relevant singularity is approached, the  $q_n$  expression in (12.11) behaves as  $q_n = \mathcal{O}(W^{-5\alpha-(1-3\alpha)(n+\gamma)})$ . Requiring it to match (12.19) with  $n = 0$  yields

$$\gamma = \frac{5\alpha}{1-3\alpha} = -\frac{5\sigma}{1+3\sigma}. \quad (12.22)$$

It remains to determine the prefactor  $\Lambda$  that appears in the form of  $Q$  in (12.17b). There is no simple analytical procedure for this; in order to calculate  $\Lambda$ , we must solve a recurrence relation. We do not present the details here but refer readers to Chapman and Vanden-Broeck [2006] and Trinh et al. [2011].

## 12.6 THE STOKES SWITCHING

The procedure for optimal truncation and derivation of the general form of the exponentials switched on follows in a somewhat generic way to procedures shown in previous chapters. The solution is expressed as an optimally truncated series and remainder, and a linear equation for the remainder is sought. The equation for the remainder is forced by the late-orders behaviour (??) and thus establishes the connection between the exponentially-small terms and the divergent series. The theory can be found in [Chapman and Vanden-Broeck, 2006, Sec. 4]. The point is that across a Stokes line, the following term switches on in  $q$ :

$$\sim \frac{2\pi i}{\epsilon^\gamma} Q e^{-\chi/\epsilon}. \quad (12.23)$$

There is one such contribution for each relevant Stokes line intersection.

## 12.7 STOKES LINES

There are two singularities that can play an important role in driving the divergence of the series and in the subsequent production of exponential switchings. Numerically, it can be confirmed that the stagnation point  $e = 0$  does not produce a significant contribution (cf §5.1 of Trinh et al. 2011), and so we shall focus on the corner point<sup>13</sup>.

<sup>12</sup>See Chapman and Vanden-Broeck [2006] or Trinh et al. [2011]. Briefly explained, we show that  $q_1 = \mathcal{O}(q_0^3 \frac{dq_0}{dw})$ . This is then used in  $Q$  to show the exponential factor in (12.17b) is  $\mathcal{O}(1/q_0^3)$ . This power of  $-3$  is combined with the power of  $-2$  in (12.17b) to form a power of  $-5$  in (12.21).

<sup>13</sup>The nature of the free-surface near the stagnation point,  $w = 0$ , is a surprisingly complex problem. First, there is the issue of how the solution behaves near  $w = 0$  at a fixed value of  $\epsilon$  (the inner problem); the works of, for example, ? and ? have examined some of these problems. Second, there is the question of how the solution near

The corner is the critical point which is responsible for the generation of waves. Since  $\chi(-1) = 0$ , we may write (12.17a) as

$$\chi = i \int_{-1}^w \frac{1}{q_0^3(\varphi)} d\varphi = i \int_{-1}^w \left( \frac{\varphi + 1}{\varphi} \right)^{3\sigma} d\varphi, \quad (12.24)$$

where the contour of integration can be taken along any path in the upper-half plane, *not* through  $w = 0$ . Near the corner,

$$q_0 \sim e^{\pi i \sigma} (w + 1)^{-\sigma} \quad \text{and} \quad \chi \sim \left[ \frac{ie^{-3\pi i \sigma}}{1 + 3\sigma} \right] (w + 1)^{1+3\sigma} \quad (12.25)$$

and from Dingle [1973], Stokes lines are expected whenever  $1 + 3\sigma > 0$ , and also

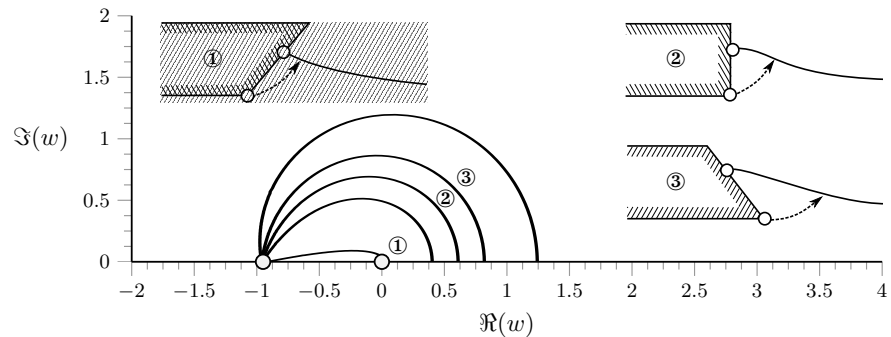
$$\text{Im}(\chi) = 0 \quad \text{and} \quad \text{Re}(\chi) \geq 0. \quad (12.26)$$

The first (and only relevant) Stokes line leaves the critical point at an angle of

$$\vartheta = \pi \left( \frac{3\sigma - 1/2}{1 + 3\sigma} \right),$$

arcs into the upper-half plane, and continues until it intersects the free-surface. This is shown in Figure 12.5. We note that as  $\sigma \rightarrow 0$ , the intersection point tends towards the origin.

Figure 12.5: Stokes lines for various hulls, such  $\sigma = 0.2$  as ①,  $\sigma = 0.4$ ,  $\sigma = 0.5$  as ②,  $\sigma = 0.6$  as ③, and  $\sigma = 0.8$ . The Stokes lines are closed loops that begin and end at  $w = -1$  and are symmetrical about the real axis. Across the intersection of the Stokes line with  $\text{Re}(w) > 0$ , we expect an exponential to switch on. Although they are an *imaginary* construct and lie on the analytically continued free-surface, they nevertheless share a correspondence with a line in the physical plane which begins at the corner and arcs towards the free-surface.



## 12.8 EXPONENTIAL SUBDOMINANCE OF THE INTEGRAL

There is a key simplification that was used in (12.14) and allowed the boundary integral to be neglected in consideration of the late terms. In order to demonstrate the late-order subdominance of the boundary integral, consider the case of  $\sigma = 1/2$  (other values of  $\sigma$  are similarly done). Here, the Stokes line originating from the corner leaves at an angle of  $2\pi/5$  in the potential plane, curves in an arc, and intersects the

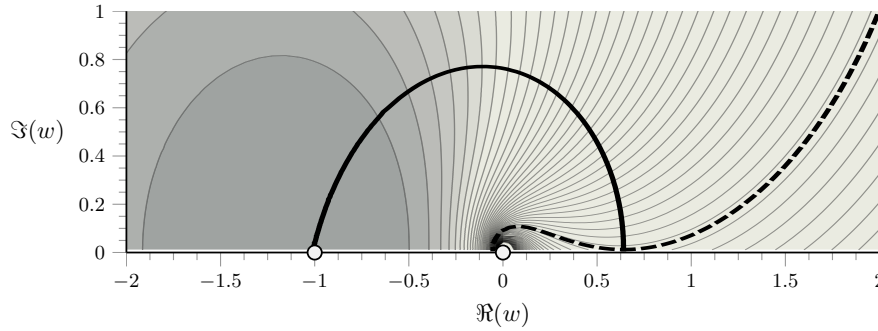


Figure 12.6: The light lines are contours for  $|\chi(w)|$ , with dark regions corresponding to small values. The thick black line corresponds to the Stokes line, and the dashed line to  $|\chi(w)| = 3\pi/2$ . Our Stokes line switching analysis is confined to the region above the dashed line, where the relevant exponentials are larger than anywhere along the free-surface.

free surface at about  $w = \phi_c \approx 0.635$ . Along the real and positive  $w$ -axis,  $\text{Re}(\chi) = 3\pi/2$ , which can be computed by the residue contribution of (12.24) at infinity.

In Figure 12.6, we plot the contours of  $|\chi(w)|$ , a thick line representing the Stokes line, as well as a dashed line for the contour  $|\chi| = 3\pi/2$ . Since  $\chi(w)$  is an analytic function away from its singularities, the contour  $|\chi| = 3\pi/2$  must necessarily intersect both the Stokes line and the real axis at the single point  $w = \phi_c$ . Moreover, along the real axis the point  $\phi_c$  constitutes an absolute minimum. For the equation

$$\frac{q_n}{q_0} + i\theta_n - \frac{q_{n-1}q_1}{q_0^2} + \dots = \mathcal{H}[\theta_n(w)],$$

when the ansatz (12.11) is used and the late terms sought, the integral will be evaluated on the real axis, where  $\chi$  is larger than on anywhere along the Stokes line. Thus the right-hand side of the equation is negligible as  $n \rightarrow \infty$ . Essentially, its main effect in the analysis is in altering the values of the early terms,  $q_0$ ,  $q_1$ ,  $q_2$ , and so on.

The subdominance of the boundary integral term which occurs in potential theory was also used for the analysis of the viscous fingering problem in Hele-Shaw flows of Chap. 13.

## 12.9 NUMERICAL VERIFICATION

### 12.10 EXTENSIONS

#### 12.10.1 Two-dimensional flows for more general bodies

#### 12.10.2 Three-dimensional flows

#### 12.10.3 Time-dependent flows

#### 12.10.4 Surface tension and other effects